Reconsidering seismological constraints on the available parameter space of macroscopic dark matter

David Cyncynates, Joshua Chiel, Jagjit Sidhu, and Glenn D. Starkman

Reconsidering seismological constraints
on the available parameter space of macroscopic dark matter

David Cyncynates, Joshua Chiel, Jagjit Sidhu and Glenn D. Starkman

Physics Department/CERCA/ISO
Case Western Reserve University
Cleveland, Ohio 44106-7079, USA

Using lunar seismological data, constraints have been proposed on the available parameter space of macroscopic dark matter (macros). We show that actual limits are considerably weaker by considering in greater detail the mechanism through which macro impacts generate detectable seismic waves, which have wavelengths considerably longer than the diameter of the macro. We show that the portion of the macro parameter space that can be ruled out by current seismological evidence is considerably smaller than previously reported, and specifically that candidates with greater than or equal to nuclear density are not excluded by lunar seismology.

I. INTRODUCTION

If General Relativity is correct, then dark matter constitutes most of the mass density of the Galaxy. Yet, decades after the case for dark matter became compelling [1] and widely accepted (although see [2]) we still do not know what it is. The most widely considered and searched for candidates are new particles not found in the Standard Model of particle physics, such as the generic class of Weakly Interacting Massive Particles (WIMPs) (especially the Lightest Supersymmetric Particle) and axions.

In this paper, we consider instead a class of macroscopic dark matter (macros) candidates. The theoretical motivation for this stems originally from the work of Witten [3], and later, more carefully Lynn, Nelson and Tetradis [4]. Macroscopic objects made of baryonic matter with sizable "strangeness" (i.e. many of the valence quarks are strange quarks, rather than the usual up and down quarks found in protons and neutrons) may be stable, and may have been formed before nucleosynthesis [3, 4], thus evading the principal constraint on baryonic dark matter. The appeal of such a dark matter candidate is that there would be no need to invoke the existence of new particles to explain the observed discrepancy between gravitational masses and luminous masses in galaxies.

Observational limits on such macroscopic dark matter have been obtained by several groups over the years. Some of these have been specific to the original "strange matter" paradigm, while others have been more phenomenological. Recently, one of us, with colleagues, presented a comprehensive assessment of limits on such macros as a function of their mass and cross-section [5], identifying specific windows in that parameter space that were as yet unprobed. We later refined those in [6]. An interesting window identified there was for macros with masses of greater than about 55g, and densities that included nuclear density. This is shown in Figure 3 of [5] reproduced here as Figure 1.

In [5], no mention was made of seismological bound on macros – obtained by considering the effects of macros striking the Earth or Moon – even though these could conceivably have intruded into the open window identified above 55g. Here we justify that caution, reconsidering the seismological signals that could be observed when such a dark matter candidate impinges on the Moon, and finding that the signal (and hence the limits on macro abundance) had been overestimated.

It has been suggested [7] that the energy deposition into the 1 Hz range from a nuclearite (nuclear-density macro) impact on the Moon or Earth should be approximately 5% of the total energy deposition. This, as shown in section II A, is a sizable overestimate even compared to our own purposefully generous estimate. We produce a more accurate model of the seismic effects of macro impacts, including in our model the effects of geometric lensing, stratification of the Moon, anelastic attenuation, and geometric attenuation. The most important consideration is that even a sizable mass macro is very small compared to the multi-kilometer wavelengths of seismic waves that propagate unattenuated through the Moon or Earth. The production of detectable long-wavelength seismic waves is therefore highly suppressed relative to short-wavelength waves.

For the balance of this paper, we focus on the Moon, rather than the Earth, as the target system. Unlike the Earth, the Moon is seismically quiet. Most internal seismological activity in the Moon originates from deep Moonquakes, which are very attenuated by the time they reach the surface.
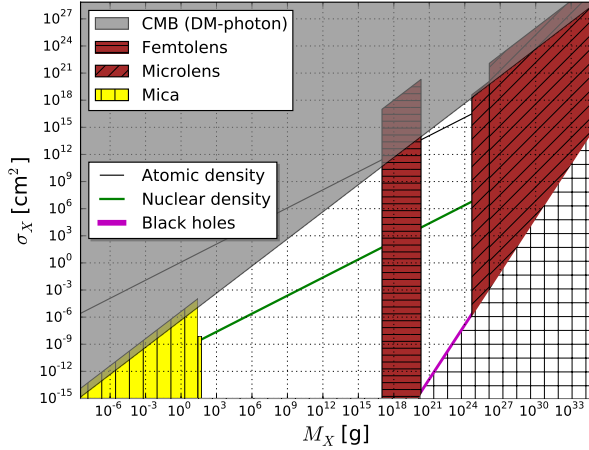
FIG. 1. Figure 3 of [5] "Constraints on the macro cross section and mass (assuming the macros all have the same mass), applicable for both elastically- and inelastically-scattering candidates. In red are the femto- and micro-lensing constraints, while in grey are the CMB-inferred constraints. The black and green lines correspond to objects of constant density 1g/cm^3 and $3.6 \times 10^{14}\text{g/cm}^3$, respectively. Black hole candidates lie on the magenta line, however, these may be ruled out for other reasons; objects within the hatched region in the bottom-right corner should not exist as they would simply be denser than black holes of the same mass." The yellow region labeled "Mica" has been excluded by etching and inspecting sheets of ancient mica. See [5] for further explanations and appropriate references.

Most of the noise in lunar seismograms comes from meteoroids, but meteoroid impacts are for the most part easily identifiable as such. This allows us to place constraints on the macro flux from the total seismic event rate. A more sensitive search for macro impacts could seek, as Teplitz *et al.* have [7], to identify the distinctive linear morphology of seismic events that a macro would cause as it bored straight through the target at high velocity (typically hundreds of km/s). We look forward to that in a future paper.

The result of the current analysis is an upper bound on the event rate that would have been measured by the Apollo lunar seismometers that substantially weakens the previously reported macro bound. In particular, we find that macros of nuclear or greater density are not constrained by lunar seismic data.

II. THE SEISMIC SOURCE

A. Seismic Wave Generation

Once a macro hits the Moon it can suffer a variety of fates. If it is comparable in density to ordinary matter, then, like a meteoroid, it will deposit all of its kinetic energy over a small distance and result in an impact crater at the lunar surface. Here, we are more interested in macro candidates that are much denser, probably comparable to nuclear density, striking the Moon with an impact speed characteristic of relative orbital speeds in the Milky Way (several hundred km/s). This is far in excess of the speed of sound in rock, which is just a few km/s.

A precise evaluation of the seismic signal resulting from such an impact would require detailed modeling of the response of lunar rocks to the passage of a hypersonic dense projectile. We will attempt below to put an upper limit on the strength of that seismic signal, and thereby demonstrate that it is difficult to place strong limits on macros from lunar seismology. We will therefore consistently *overestimate* the seismic signal.

Because of the hypersonic impact of the macro, we expect a good model of the initial effect of its passage through the rock to be the instantaneous heating of all the rock in a column swept out by the cross-section σ_X of the macro. We approximate this as each atom of rock material acquiring a random velocity approximately equal in magnitude to the impact velocity of the macro. The macro therefore deposits energy along a straight line through the Moon at a rate

$$\frac{dE}{dx} = \rho_{\text{Moon}} \sigma_X v_X^2 \,. \tag{1}$$

A macro of mass M_X will therefore traverse the Moon without significant deceleration if

$$2R_{\text{Moon}} \sigma_X \rho_{\text{Moon}} \ll M_X \,, \tag{2}$$

where ρ_{Moon} is the appropriately averaged lunar density and $2R_{\text{Moon}}$ is the lunar diameter. For the balance of this paper, we will take equation (2) to apply, unless specifically noted.

This energy deposition transforms the impacted rock into a column of ionized plasma, and initiates an outward propagating melt front. We show in appendix A below that for the macro cross-sectional areas of interest to us, the melt front either advances subsonically immediately, or at best the transition from supersonic to subsonic propagation occurs marginally outside the macro radius. Once the

velocity of the melt front becomes subsonic, a seismic wave, sourced by the overpressure interior to the melt front, will begin to propagate radially outward ahead of the melt front.

Initially the outgoing wave will be non-linear, and will likely also result in the fracturing of the rock. Eventually, the pressure amplitude of the wave will fall below p_0, the maximum differential pressure that the rock in this region can support elastically. From this time forward, we can treat the outgoing seismic wave as an ordinary linear wave.

We begin by estimating the energy carried in that outgoing wave. Taking the column of overpressured melted rock to be instantaneously generated, the resulting overpressure will be radially symmetric and of the form

$$p(r) = \begin{cases} p_0 f(r) & \text{if } a < r < b, -\frac{\ell}{2} < z < \frac{\ell}{2}, \\ p = 0 & \text{otherwise,} \end{cases} \quad (3)$$

where $0 < f(r) < 1$. The overpressure extends over the entire length of the column ($-\ell/2 < z < \ell/2$) over some range of radii $a < r < b$. After a short time, the pressure will remain in this cylindrically symmetric form (at least away from the lunar surface), since the inhomogeneity of the Moon (and hence of the development of the evolving pressure distribution) is significant only on scales of tens or hundreds of kilometers.

The energy of a seismic p-wave is

$$E = \frac{1}{2} \int d^3 x \left(\rho |\partial_t u|^2 + (\lambda + 2\mu)|\nabla u|^2 \right), \quad (4)$$

where u is the displacement field, and ρ, λ, μ are the density and Lamè coefficients respectively. For p-waves, $p = -K\nabla \cdot u$ where K is the bulk modulus.

We can rewrite (4) in terms of the Fourier transform of $p(r)$. To leading order in kb this is

$$P = \frac{4\pi p_0}{k \cos\theta} \sin\left(\frac{\ell k \cos\theta}{2}\right) F + \mathcal{O}((kb)^0), \quad (5)$$

where k is the magnitude of the wave-vector, θ is the angle the wave-vector makes with the tube axis, and $F \equiv b^2 f_1(b) - a^2 f_1(a)$, where

$$f_1(r) = \sum_{n=0}^{\infty} \sum_{m=0}^{n} \binom{n}{m} \frac{f^{(n)}(r_0)}{n!} \frac{(-r_0)^{n-m}}{2+m} r^m, \quad (6)$$

for any choice of $r_0 \in [a, b]$. The form of (6) follows when we Taylor expand $f(r)$ and apply the binomial theorem.

Defining $\kappa \equiv K^2/(\lambda + 2\mu)$, it follows that

$$E = \frac{1}{\kappa} \int \frac{d^3 k}{(2\pi)^3} |P|^2. \quad (7)$$

The seismometers that were left on the Moon by the Apollo astronauts, and which functioned until being decommissioned in 1977, were sensitive at frequencies up to $20\,\text{Hz}$ to displacements as small as $0.3\,\text{nm}$ [8, 9]. The detectable energy is therefore

$$E_k = \frac{1}{\kappa} \int_0^k \frac{dk'\, d\theta}{(2\pi)^2} k'^2 \sin\theta |P|^2$$

$$= \frac{2p_0^2 F^2 k^2 \ell}{\kappa} \left[\frac{\sin(k\ell) + k\ell(\cos(k\ell) - 2)}{k^2\ell^2} + \text{Si}(k\ell) \right]$$

$$+ \mathcal{O}((kb)^4).$$

Note that

$$\frac{\pi}{2} \leq \frac{\sin(x) + k\ell(\cos(x) - 2)}{x^2} + \text{Si}(x) \leq \frac{\pi}{2} + \frac{4}{x},$$

so, when $k\ell \gg 4$ we have

$$E_k \simeq \frac{1}{\kappa} \pi \ell p_0^2 F^2 k^2 \equiv C_1 k^2. \quad (8)$$

The initial pressure profile is probably determined by the details of the initial macro-induced plasma, and the subsequent outward propagation of a melt front. As described above, once that front propagates out subsonically, a seismic p-wave will travel outward from the column of molten rock. Initially, however, the overpressures in the wave may be outside the linear regime for the rock elasticity. As the pressure wave propagates outward, it is attenuated until the pressure differential is within the linear regime.

The macro travels hypersonically and will generate a shock wave. Shock waves typically evolve to pressure fronts resembling a right triangle [10], i.e. $f = (r - r_0)/\Delta r$ where $a = r_0$ and $b = r_0 + \Delta r$. We adopt this shape also for its simplicity, in the expectation that the specific shape is unlikely to grossly alter the conclusions. In this case $f_1(r) = (2r - 3r_0)/6\Delta r$ and

$$E_k = \frac{\Delta r^2 (3r_0 + 2\Delta r)^2}{36\kappa} \pi \ell p_0^2 k^2. \quad (9)$$

The total energy of the pressure wave is (from (4))

$$E = \frac{2\pi p_0^2 \ell}{\kappa} \int_a^b r\, dr f(r)^2,$$

$$= \frac{p_0^2}{6\kappa} \pi \Delta r \ell (4r_0 + 3\Delta r).$$

Some of that energy would be lost to structural changes to the rock, such as melting and breaking. The non-linear regime is characterized by faulting

3

and fracturing. Brittle failure for granite occurs at a stress exceeding 3×10^8 Pa [11], which is much less than the initial overpressure that the macros will leave behind in their melt tubes. By ignoring dissipation during the non-linear evolution of the seismic waves, we will, as intended, overestimate the energy that would reach the seismometers. Overestimating the signal, we set $E = \rho \sigma_X \ell v_X^2 \equiv \epsilon \ell$, take $p_0 = \min\left(10^8\,\text{Pa}, p_{\text{source}}\right)$, and obtain an expression for r_0, which demarcates the end of the non-linear regime:

$$r_0 = \frac{3\kappa\epsilon}{2\pi p_0^2 \Delta r} - \frac{3\Delta r}{4}\,. \tag{10}$$

The fraction of the original deposited energy detectable to seismometers is thus

$$\Xi \equiv \frac{E_k}{E} = k^2 \frac{\left(\pi p_0^2 \Delta r^2 - 18\kappa\epsilon\right)^2}{576\pi p_0^2 \kappa\epsilon}\,. \tag{11}$$

A lower bound on r_0 is 0, corresponding to linear behavior from the start. (Actually, the lower bound is $\sqrt{\sigma_X/\pi}$, but the difference is negligible.) This, in turn, imposes an upper bound on the pulse width

$$\Delta r \leq \sqrt{\frac{2\kappa\epsilon}{\pi p_0^2}}\,. \tag{12}$$

When Δr is restricted to its physical range, Ξ is a monotonic decreasing function in Δr. Thus, replacing Δr with its extremal values, we obtain the following bounds on Ξ,

$$\frac{4}{9}\frac{\kappa\epsilon k^2}{\pi p_0^2} \leq \Xi < \frac{9}{16}\frac{\kappa\epsilon k^2}{\pi p_0^2}\,. \tag{13}$$

It is important to note that these expressions only hold for $k(r_0 + \Delta r) \ll 1$, however they will always provide an over-estimate of the fraction of detectable energy. Moreover, this condition holds for a wide variety of relevant parameters. Taking $\rho = 3.3 \times 10^3\,\text{kg m}^{-3}$, $v_X = 2.5 \times 10^5\,\text{m s}^{-1}$, $\kappa = 5.5 \times 10^{10}\,\text{Pa}$, and $k = 1.5 \times 10^{-2}\,\text{m}^{-1}$ [12], we obtain $\Xi < 4.5 \times (\sigma_X/\text{cm}^2)$. To obtain the 0.05 that Teplitz *et al.* used, one must take $\sigma_X > 10^{-2}\,\text{cm}^2$, which is rather large [13] (cf. Figure 1).

The choice of $p_0 = 10^8$ Pa does significantly impact our result; ultimately the measured displacements we calculate will be inversely proportional to p_0. Our choice of p_0, however, is well below the overpressure corresponding to the boundary between linear and non-linear elasticity in the Moon. As the ambient pressure on a sample of rock increases, so

too does p_0 [14–16]. We have taken p_0 to be a factor of 3 below that of granite with a modest 50 MPa overpressure [11]. In reality, p_0 is probably, on average, orders of magnitude larger than we claim it to be because the ambient pressure in the Moon is on the order of GPa rather than MPa. This is one more way in which we overestimate the seismic signal.

To our knowledge, no measurements probe the elastic behavior of rock at these high pressures. Note also that this choice of p_0 corresponds to r_0 on the order of 1 km, which well exceeds the regime of non-linearity we would have expected based on the solutions to the heat equation (Appendix A).

III. SEISMIC WAVE PROPAGATION

The velocity of p-waves as a function of distance r from the center of the Moon (or the Earth, and presumably other spherical rocky celestial bodies) is of the form $v(r) = a^2 - b^2 r^2$ [12, 17] in each of a number of layers. Using Snell's law, we obtain the differential equations for the trajectory of p-wave rays within each layer

$$v^2 = \dot{r}^2 + \frac{p_{\text{ray}}^2 v^4}{r^2}\,,$$

$$\dot{\theta} = \pm \frac{p_{\text{ray}} v^2}{r^2}\,.$$

where θ is the polar angle of the ray measured from the center of the Moon, and p_{ray} is the ray parameter, which is fixed along any given ray trajectory. These equations can be integrated with the above $v(r)$ to obtain, for some constants q and θ_0,

$$r(t) = \frac{a\sqrt{(qe^{2abt} - b)^2 + 4a^2 b^4 p_{\text{ray}}}}{b\sqrt{(qe^{2abt} + b)^2 + 4a^2 b^4 p_{\text{ray}}}}\,,$$

$$\tan(\theta(t) - \theta_0) = \frac{q^2 e^{4abt} - b^2}{4ab^3 p_{\text{ray}}} + abp_{\text{ray}}\,.$$

The Moon, like the Earth, is stratified. At each boundary, a ray will be reflected and transmitted. We assume for simplicity that the reflection and transmission coefficients are frequency independent. While this may lead to either an overestimate or an underestimate of the signal, the net effect of these reflections and transmissions on the limit is small, and so their frequency dependence is unlikely to spoil the overall point.

The last effect to account for is anelastic attenuation (i.e. absorption), characterized by the quality factor Q, which depends on both frequency and r For

a given mode, the ratio of final to initial amplitude is

$$\exp\left[-k\int_{t_0}^{t}\mathrm{d}t'\frac{v(r(t'))}{2Q(r(t'))}\right]\equiv\exp\left[-k\mathscr{D}\right].\quad(14)$$

The VPREMOON Model [12] provides piecewise-constant data for Q, so it is reasonable to subdivide the Moon further into strata of different Q. For propagation within a given layer i, the factor $\mathscr{D}$ is given by $\Delta t_i v_i/2Q_i$, where we take v_i to be the average velocity within that stratum. For the case of the Moon (and the Earth), this is a good approximation, since v doesn't change significantly within a given layer of constant Q. Again, while this approximation may lead to either an overestimate or an underestimate of the signal, the net effect of the attenuation on the limit is small, because we are interested only in long wavelength modes which have less attenuation.

Thus, the amplitude of a ray can be computed by knowing the two numbers

$$\mathscr{T}\equiv\prod_i\mathscr{T}_i\,,$$

$$\mathscr{D}\equiv\sum_i\frac{\Delta t_i v_i}{2Q_i}\,,$$

where $\mathscr{T}_i$ are the reflection or transmission coefficients at boundary i on which the ray is incident.

IV. SEISMIC WAVE DETECTION

Consider a p-wave traveling towards positive x, and with amplitude that is non-zero only within some region S in the plane normal to to its motion. Denote $A\equiv\int_S\mathrm{d}y\,\mathrm{d}z$, and let χ_S be 1 on S and 0 elsewhere. The displacement field of the wave is

$$u(\vec{x},t)=\chi_{\mathbb{R}\times S}\int\frac{\mathrm{d}k}{2\pi}U(k)e^{-\mathrm{i}k(x-v_pt)},\quad(15)$$

so

$$|u(\vec{x},t)|\leq\int\frac{\mathrm{d}k}{2\pi}|U(k)|\,.\quad(16)$$

Its energy is

$$E=\rho v_p^2 A\int\frac{\mathrm{d}k}{2\pi}k^2|U(k)|^2\,.\quad(17)$$

As before, we denote the energy in the low frequency spectrum

$$E_k=\rho v_p^2 A\int_0^k\frac{\mathrm{d}k'}{2\pi}k'^2|U(k')|^2\,.\quad(18)$$

It follows that

$$|U(k)|=\sqrt{\frac{2\pi}{\rho v_p^2 A}}\frac{1}{k}\sqrt{\frac{dE_k}{dk}}\,,\quad(19)$$

and from the estimate above (16)

$$|u(\vec{x},t)|\leq(2\pi\rho v_p^2 A)^{-1/2}\int_0^k\frac{\mathrm{d}k'}{k'}\sqrt{\frac{dE_{k'}}{dk'}}\,.\quad(20)$$

In our case $E_k=\Xi E=C_1 k^2$ before attenuation. After anelastic attenuation, $dE_k/dk=2\mathscr{T}C_1 ke^{-k\mathscr{D}}$

$$|u(\vec{x},t)|\leq\sqrt{\frac{2}{\rho v_p^2 A}}\sqrt{\frac{\mathscr{T}\,\Xi E}{\mathscr{D}}}\frac{1}{k}\mathrm{Erf}\left[\sqrt{\frac{\mathscr{D}k}{2}}\right]\,.\quad(21)$$

No similar simple analytic expression emerges when E_k includes the energies of two or more different rays, each with different attenuation factors. If attenuation were important, we could average $\mathscr{D}$ among the coincident rays and obtain an approximate upper bound on $|u(\vec{x},t)|$. However, since we only wish to consider the lowest frequency modes, $f<20$ Hz, and $\mathscr{D}k\ll 1$, so absorption does not significantly alter u. Taking $k\mathscr{D}=0$, the displacement caused by the incident p-wave is bounded above by

$$|u(\vec{x},t)|\leq\sqrt{\frac{4\mathscr{T}\,\Xi E}{\pi k\rho v_p^2 A}}\,.\quad(22)$$

V. SIMULATION

In previous works (e.g. [7]), homogeneous Earth and Moon models have been used to constrain the parameter space of macroscopic dark matter. This approach neglects the lensing that occurs because of the velocity gradient and the spherical boundaries of strata, as well as the energy losses from reflection and refraction across these boundaries. Here, we propagate rays, each carrying a fraction of the total energy deposited by the macro, from the macro's original line of impact to the boundary of the Moon. We then create an intensity map of the lunar surface for a representative sample of macro impacts. Finally, we convert the intensity maps to displacement maps, and using the sensitivity of the lunar seismometers, we obtain an average event rate that the lunar seismometers would measure.

A. Data Generation

We consider a macro trajectory that passes a distance D from the lunar center. The trajectory has

some length L within the moon, which we sample at M points. From each point we propagate N randomly oriented rays, each endowed with energy $E_i = \rho(r_i)\sigma_X v_X^2 L/(MN)$, where $i \in \{1, \ldots, M\}$ labels the points. We use the trajectories derived in section III to propagate the rays. Because of the approximation of spherical symmetry, each ray propagates in a plane.

Since the moon is stratified, we split the propagation of a ray at the boundary of each layer into a reflected and a transmitted ray. During a ray's propagation through a given stratum, its time spent in that layer Δt_i, the attenuation factor in that layer $\mathscr{D}_i$, and the reflection/transmission coefficient $\mathscr{T}_i$ are all recorded. Each time a ray reaches the surface of the Moon, its position, cumulative propagation time Δt and other trajectory attributes are recorded. In this full model, it would take 16 iterations to propagate a ray from one side of the moon to the other. Since Q is nearly constant, we reduce the number of boundaries by taking $Q = 6750$. In this case, it takes 8 iterations to propagate through the Moon. We expect this to lead to an overestimate of the signal, since each encounter with a boundary reduces the amplitude of the wave that reaches the surface.

B. Data Analysis

To analyze the simulations, we convert the surface-incident ray position data to HEALPix pixelization [18]. (We use $n_{\text{side}} = 16$). The area of a HEALPix pixel is $A_{\text{pix}} = 4\pi R_{\text{moon}}^2/n_{\text{pix}}$, where $n_{\text{pix}} = 12 \times n_{\text{side}}^2$. A seismic wave can therefore cross a HEALPix pixel on the surface in $t_{\text{crossing}} \simeq \sqrt{A_{\text{pix}}/\pi v_{\text{surface}}^2}$. According to [12], $v_{\text{surface}} \simeq 1 \, \text{km s}^{-1}$. Rays that reach a surface pixel within t_{crossing} of one another are taken to add constructively.

We distribute the energy of each ray evenly over its pixel, and thus set A (as in equation (17) and following) equal to A_{pix}. This is a good approximation when $N = n_{\text{pix}}$, since the average angular separation of the rays at the source corresponds to the average angular separation of the HEALPix pixels. We omit the effects of anelastic attenuation, as inspection of the propagation data showed that typically $k\mathscr{D} \simeq 10^{-2}$ for the frequencies of interest in the Moon.

Using (22), we compute an upper bound for the displacement within a given surface pixel, and compare that to the sensitivity of the lunar seismometers given in [8]. If the calculated displacement is less than the seismometer sensitivity, then the seismic wave is considered undetectable in that pixel. The number of detectable pixels is denoted m_D, for a macro making closest approach D to the lunar center.

It is unlikely that a macro impact will be detected if it only just exceeds the seismometer sensitivity in one seismometer. As the displacement approaches $d_{\text{min}} = 3 \times 10^{-10}$ m in a pixel with a seismometer, we should expect no chance of detection, while as $d \to \infty$ the impact should always be detected. We model this by taking the probability of detecting a seismic signal with displacement Δx_i in the ith surface pixel (if it contains a seismometer) to be

$$m_{D,i} \equiv \max\left\{0, 1 - \exp\left[p\left(1 - \frac{\Delta x_i}{d_{\text{min}}}\right)\right]\right\}. \quad (23)$$

Here p describes how the detection probability increases as the strength of signal increases. (For example, if $\Delta x = 4d_{\text{min}}$ is q times as detectable as $\Delta x = 2d_{\text{min}}$, then $p = \ln\sqrt{q}$.) Summing over all the pixels yields the effective number of pixels in which there exists a detectable signal

$$m_D = \sum_{i=1}^{n_{\text{pix}}} m_{D,i}. \quad (24)$$

In the end, we take $p \to \infty$ so as to, once again, overestimate the probability of detecting a lunar macro impact.

This procedure is repeated for 20 values of the impact parameter D, evenly spaced by 85 km. The average number of pixels on which there exists a detectable signal is then

$$m = \frac{\sum_D D m_D}{\sum_D D}. \quad (25)$$

If there are n lunar seismometers (or tight clusters thereof), we suppose that each occupies one HEALPix pixel. If $n + m \geq n_{\text{pix}}$, then detection is guaranteed. Otherwise, if $\mathcal{M}$ macros impact the moon, the likelihood of any of them being detected is

$$\mathcal{P} = 1 - \left[\frac{(n_{\text{pix}} - n)!(n_{\text{pix}} - m)!}{n_{\text{pix}}!(n_{\text{pix}} - n - m)!}\right]^{\mathcal{M}}. \quad (26)$$

$\mathcal{P}$ is a function of σ_X, but not of M_X.

VI. RESULTS

We have taken $p = \infty$ in (24) when calculating m_D, so as to overestimate the signal. The resulting

detection probability versus macro cross-section is plotted in Figure 2. A very good fit to the curve is

$$\mathcal{P}(\sigma_X) \simeq \text{Erf}[(\sigma_X/\sigma_0)^2(1 + \sigma_X/\sigma_1)] \qquad (27)$$

with $\sigma_0 = 4.67 \times 10^{-7} \text{cm}^{-2}$ and $\sigma_1 = 2.17 \times 10^{-8} \text{cm}^{-2}$. There is thus a very clear transition around $\sigma_X \simeq 10^{-7}$ cm^2 where the detection probability increases rapidly with increasing cross-section.

Using the computed detection probability $\mathcal{P}(\sigma_X)$, and the flux of macros impinging on the Moon

$$\Phi(M_X) \simeq 5 \times 10^7 (M_X/\text{ g})^{-1} \text{ yr}^{-1}, \qquad (28)$$

we can determine which values in the σ_X vs. M_X parameter plane could be excluded using the Apollo seismometer data. The reported rate of seismic events detected on the Moon by the four (clusters) of Apollo seismometers was 2500 events per year. Therefore a good approximation of the excluded region is

$$\mathcal{P}(\sigma_X)\Phi(M_X) > 2500. \qquad (29)$$

(If one had confidence that at most some fraction f of these could be macros, then for fixed M_X one could improve the constraint on σ_X but only by at most $f^{1/2}$, due to the functional form of $\mathcal{P}(\sigma_X)$.)

In Figure 3, we reproduce Figure 3 of [5] (i.e. Figure 1) with the "exclusion region" defined by (29) shaded blue. For $M_X > 2 \times 10^4$g, the flux of macros is too low to give the observed seismic event rate; below the region, the energy deposited is too small for the events to be detected. Since our calculation assumed that the macro passed through the entire moon without significant slowing, it applies only for $M_X > \sigma_X \rho_{\text{Moon}} 2R_{\text{Moon}}$, which forms the upper boundary of the solid blue limit. However, for fixed M_X, increasing σ_X above $M_X/(\rho_{\text{Moon}} 2R_{\text{Moon}})$ seems unlikely to significantly reduce the signal, since the total energy deposited will remain fixed but along a shorter path, nearer the lunar surface. We thus expect the region above the solid blue region to be excluded as well, and cross hatch it in blue.

We emphasize that since we have consistently overestimated the detectability of the signal, the actual excluded region of parameter space lies above the shaded region (i.e. at higher σ_X for any given M_X).

VII. CONCLUSION

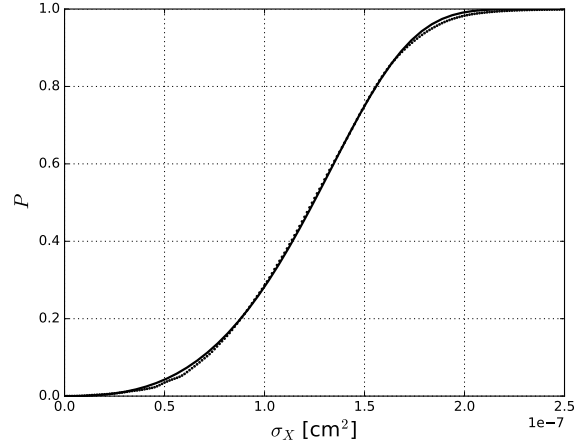We have considered more carefully than in the past the seismic signal generated by a macroscopic

FIG. 2. Detection Probability versus Cross-Section. The curve of best fit (solid) plotted is of the form $\text{Erf}[(\sigma_X/\sigma_0)^2(1 + \sigma_X/\sigma_1)]$ with $\sigma_0 = 4.67 \times 10^{-7}\text{cm}^{-2}$ and $\sigma_1 = 2.17 \times 10^{-8}\text{cm}^{-2}$.
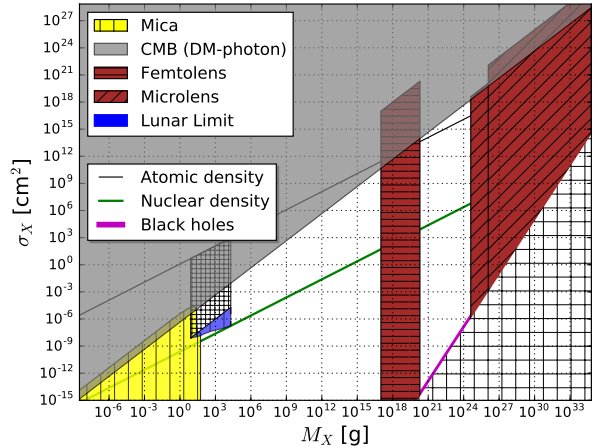

FIG. 3. Figure 3 of [5] with the maximum seismic "excluded" region added in blue. To the right of the blue region, the event rate is too low because the macro flux is too low; below the region, the signal strength is definitely too low. The excluded region is divided in two. In the solid blue colored region, our calculations apply. In the hatched region above it, the macro stops inside the moon and our calculations are not valid, but we expect this region is excluded as well. We note that the nuclear-density line lies outside the excluded region. Since we have consistently overestimated the signal, the true exclusion area from total lunar seismic rate must lie *above* the lower boundary of the blue shaded area.

dark matter candidate incident on the Moon. We have found that the signal is weakened compared to prior expectations, in particular by the mismatch between the small size of the macro and the long wavelength of the modes that propagate largely unattenuated (and to which the lunar seismometers were sensitive). For macroscopic dark matter of density greater than or equal to approximately nuclear density we have found that one cannot infer limits from the existing data on the total lunar seismological event rate.

The Earth and the Moon are ideal targets for looking for macros, whose vast surface area is difficult to improve upon. However, in order to forecast the sensitivity of future seismological searches, or to interpret future data, it will be necessary to markedly improve our understanding of how, and with what efficiency, macro kinetic energy gets transferred into detectable seismic waves.

Appendix A: Propagation of the melt front

When a macro impacts the Moon, the rock nearby is rapidly ionized, vaporized, or melted depending on its proximity to the macro. The energy deposition into these changes of phase will not contribute to primary seismic wave generation. The expansion of the radius from the macro trajectory to the boundary of the melted rock, the "melt-front," slows down with time. When the melt-front velocity is below the speed of sound, seismic waves will escape the melted region, the "melt-zone". These seismic waves carry away energy that has not already been used in phase transitions. Because we are interested in an upper bound on the seismic activity of macro impacts, we assume that the all the remaining energy propagates away as seismic waves.

Nuclear dense macros have cross-section σ_X small enough that they are reasonably approximated by a delta source. The $t = 0$ temperature field is fixed by equating the heat energy with the macro energy

$$T(r,0) = |\frac{dE}{dx}|\frac{\sigma_X}{2\pi\rho\sigma_X c_p}\frac{\delta(r)}{r} = \frac{\sigma_X v_X^2}{2\pi c_p}\frac{\delta(r)}{r}\,, \quad \text{(A1)}$$

where $|\frac{dE}{dx}|$, v_X, c_p, ρ are the energy deposition, macro velocity, impacted material heat capacity and density respectively. The temperature field then evolves into a Gaussian in r,

$$T(r,t) = \frac{\sigma_X v_X^2}{4\pi\alpha c_p}\frac{e^{-\frac{r^2}{4t\alpha}}}{t}\,. \quad \text{(A2)}$$

Setting $T(r,t) = T_{\text{melt}}$ yields an expression for the melt-radius,

$$r_{\text{m}}(t) = \sqrt{4t\alpha \ln{[C/t]}}\,, \quad \text{(A3)}$$

where

$$C = \frac{v_X^2 \sigma_X}{4\pi c_p \alpha T_{\text{melt}}}\,. \quad \text{(A4)}$$

The melt-radius velocity is then

$$\dot{r}_{\text{m}}(t) = \sqrt{\frac{\alpha}{t}}\left[(\ln{[C/t]})^{1/2} - (\ln{[C/t]})^{-1/2}\right]\,. \quad \text{(A5)}$$

For sufficiently small $t \ll C$ it is a reasonable approximation to take

$$\dot{r}_{\text{m}}(t) \approx \sqrt{\frac{\alpha}{t}\ln{[C/t]}}\,. \quad \text{(A6)}$$

We can solve for t such that $\dot{r}_{\text{m}} = v_p$, the speed of longitudinal waves, and hence determine the radius r_{fm} at which the melt wave propagation slows to less than the speed of sound,

$$r_{\text{fm}} = A\,W\left[Dr_X^2\right]\,, \quad \text{(A7)}$$

where W is the Lambert W function,

$$D = \frac{v_X^2}{c_p T_{\text{melt}} A^2} \quad \text{and} \quad A = \frac{2\alpha}{v_p}\,. \quad \text{(A8)}$$

There is a critical value of r_X, $r_c \equiv -A\,W[-(A^2 D)^{-1}]$ (where one takes the lower

branch of W) above which this calculation yields $r_{\text{fm}} < \sqrt{\sigma_X/\pi}$, which is unphysical. For $r_X > r_c$, we should take $r_{\text{fm}} = \sqrt{\sigma_X/\pi}$. For both granite ($\alpha \approx 10^{-6}\text{m}^2/\text{s}$, $T_{\text{melt}} = 1.49 \times 10^3\text{K}$ and $c_p = 1.05 \times 10^3\text{J/kg K}$ [19]) and limestone ($\alpha \approx 10^{-6}\text{m}^2/\text{s}$, $T_{\text{melt}} = 2.87 \times 10^3\text{K}$ and $c_p = 1.04 \times 10^3\text{J/kg K}$ [20]), using $v_p = 8 \times 10^3\text{m/s}$ from the VPREMOON model [12], and macro velocity $v_X = 2.5 \times 10^5\text{m/s}$, we find $r_c \simeq 3 \times 10^{-9}\text{m}$. For nuclear-density macros of the allowed masses ($M_X > 55$ g), $r_c \lesssim \sqrt{\sigma_X/\pi}$, so the melt zone is negligible, though this might not

be so for some higher density candidate macros.

Additional peculiarities with modeling the macro melt-zone are that the steep temperature gradient is not well approximated by the linear heat equation, and that the material properties of the rocks themselves are not constant in temperature. As we do not trust our model to accurately predict the energy lost, we overestimate the signal by assuming that the macro deposits all its energy into seismic waves. However, if we did use the results of this analysis, the energy loss it predicts is many orders of magnitude less than the total energy deposition, so it is inconsequential.

[1] V. C. Rubin, N. Thonnard, and W. K. Ford, Jr., Astrophys. J. **238**, 471 (1980).
[2] F. Lelli, S. S. McGaugh, and J. M. Schombert, (2016), arXiv:1606.09251 [astro-ph.GA].
[3] E. Witten, Phys. Rev. **D30**, 272 (1984).
[4] B. W. Lynn, A. E. Nelson, and N. Tetradis, Nucl. Phys. **B345**, 186 (1990).
[5] D. M. Jacobs, G. D. Starkman, and B. W. Lynn, Mon. Not. Roy. Astron. Soc. **450**, 3418 (2015), arXiv:1410.2236 [astro-ph.CO].
[6] D. M. Jacobs, G. D. Starkman, and A. Weltman, Phys. Rev. **D91**, 115023 (2015), arXiv:1504.02779 [astro-ph.CO].
[7] W. B. Banerdt, T. Chui, E. T. Herrin, D. Rosenbaum, and V. L. Teplitz, in *The Identification of Dark Matter* (2005) pp. 581–586.
[8] G. Latham, M. Ewing, J. Dorman, Y. Nakamura, F. Press, N. Toksőz, G. Sutton, F. Duennebier, and D. Lammlein, The Moon **7**, 396 (1973).
[9] Y. Nakamura, G. V. Latham, and H. J. Dorman, in *Lunar and Planetary Science Conference Proceedings*, Vol. 13 (1982) p. 117.
[10] J. W. Forbes, *Shock wave compression of condensed matter: a primer* (Springer Science & Business Media, 2013).
[11] D. A. Lockner and N. M. Beeler, International Geophysics **81**, 505 (2002).
[12] R. F. Garcia, J. Gagnepain-Beyneix, S. Chevrot, and P. Lognonné, Physics of the Earth and Planetary Interiors **188**, 96 (2011).
[13] Note that $p_0 \to 0$ does not imply $\Xi \to \infty$, since p_0 is implicitly a function of ϵ when $p_0 < 10^8$ Pa. In this case, the ratio ϵ/p_0^2 is always finite since $\epsilon \propto p_0^2$.
[14] K. Mair, S. Elphick, and I. Main, Geophysical Research Letters **29** (2002).
[15] M. Shimada, Tectonophysics **217**, 55 (1993).
[16] A. Ord, Pure and Applied Geophysics **137**, 337 (1991).
[17] A. M. Dziewonski and D. L. Anderson, Physics of the earth and planetary interiors **25**, 297 (1981).
[18] K. M. Górski, E. Hivon, A. J. Banday, B. D. Wandelt, F. K. Hansen, M. Reinecke, and M. Bartelmann, Astrophys. J. **622**, 759 (2005), astro-ph/0409513.
[19] E. C. Robertson, *Thermal properties of rocks*, Tech. Rep. (US Geological Survey,, 1988).
[20] K. Oglesby, P. Woskov, H. Einstein, and B. Livesay, *Deep Geothermal Drilling Using Millimeter Wave Technology. Final Technical Research Report*, Tech. Rep. (Impact Technologies LLC, Tulsa, OK (United States), 2014).